JCTC Journal of Chemical Theory and Computation

Article

pubs.acs.org/JCTC

Optical Signatures of OBO Fluorophores: A Theoretical Analysis

Siwar Chibani,[†] Azzam Charaf-Eddin,[†] Benedetta Mennucci,*[,‡] Boris Le Guennic,*[,§] and Denis Jacquemin*[,†,∥]

[†]Laboratoire CEISAM, UMR CNRS 6230, Université de Nantes, 2 Rue de la Houssinière, BP 92208, 44322 Nantes Cedex 3, France

[‡]Department of Chemistry, University of Pisa, Via Risorgimento 35, 56126 Pisa, Italy

[§]Institut des Sciences Chimiques de Rennes, UMR 6226 CNRS-Université de Rennes 1, 263 Av. du General Leclerc, 35042 Rennes Cedex, France

[∥]Institut Universitaire de France, 103 bd Saint-Michel, F-75005 Paris Cedex 05, France

Supporting Information

ABSTRACT: Dioxaborines dyes, based on the OBO atomic sequence, constitute one promising series of molecules for both organic electronics and bioimaging applications. Using Time-Dependent Density Functional Theory, we have simulated the optical signatures of these fluoroborates. In particular, we have computed the 0−0 energies and shapes of both the absorption and the emission bands. To assess the importance of solvent effects three polarization schemes have been applied within the Polarizable Continuum Model: the linear-response (LR), the corrected linear-response (cLR), and the state-specific (SS). We show that the SS approach is unable to yield consistent chemical trends for these challenging compounds that combine charge-transfer and cyanine characters. On the contrary, LR and cLR are more effective in reproducing chemical trends in OBO dyes. We have applied our computational protocol not only to analyze the signatures of existing dyes but also to design structures with red-shifted absorption and emission bands.

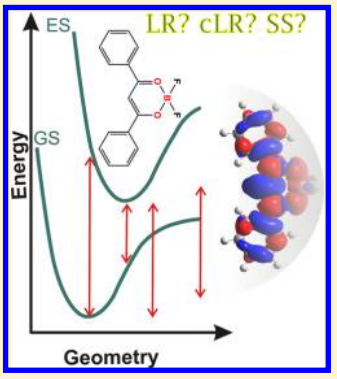

1. INTRODUCTION

Luminescent organic dyes, such as BODIPY, aza-BODIPY, and boranil derivatives, that can all be viewed as constrained cyanines have become key tools for biological, medicinal and analytical applications due to their excellent photophysical properties (see Scheme 1).[1−3] Indeed, these difluoroboron complexes have found widespread applications in several fields, for example, ion sensing,[4,5] nonlinear optics,[6] photodynamic therapy,[7] as well as biomedical indicators and fluorescence imaging.[8,9] Along with their large luminescent quantum yields, sometimes in the NIR range, their high photostability[1,2,10] and their tunable Stokes shifts might explain these successes.

Scheme 1. Representation of the Cores of BODIPY (left), Aza-BODIPY (middle), and Boranil (right)

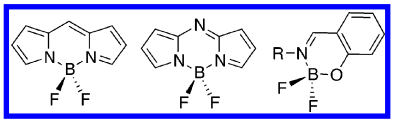

In fact, fluoroborate fluorophores can be classified into major categories depending on their atomic sequence: NBN, NBO, or OBO-bidentate ligands have indeed been proposed. The latter compounds, which are the focus of this work, present several molecular architectures (see Scheme 2).[11−44] The compounds shown in Scheme 2 have absorption and emission wavelengths spanning the 350−550 nm window [see Table S-I in the Supporting Information (SI)]. To effectively predict the optical signatures of OBO dyes, theoretical chemistry can be a handy tool. In that framework, Time-Dependent Density Functional Theory (TD-DFT) is considered as one of the most efficient approaches in terms of balance between accuracy and computational cost.[45,46] It also stands as the only first principle method tractable for simulating the optical spectra of extended molecules in condensed phase. In addition to countless studies having relied on the vertical TD-DFT approximation and aiming at establishing qualitative comparisons between vertical transition energies and experimental λ_{max}, an increasingly large number of investigations have focused on the calculations of both the 0−0 energies (E^{0-0}) and band shapes, which allow more sound comparisons with experiment.[47−54] In practice, the difference between 0−0 and vertical simulations is the necessity to optimize the geometry of the excited-state, as well as to calculate the Zero Point Vibrational Energies (ZPVE) of both states. The E^{0-0} data allow straightforward comparisons with the intersection of the absorption and emission spectral curves (experimental E^{AFCP}: absorption/fluorescence crossing point).[48]

To the best of our knowledge, no previous TD-DFT calculations have been performed to simulate the 0−0 energies nor to determine the shape of the optical spectra of OBO dyes. In fact, only three previous theoretical works devoted to OBO could be found.[14,24,25] The first study[14] aimed to determine the vertical electron affinities and intramolecular reorganization

Received: November 15, 2013
Published: January 6, 2014

   dx.doi.org/10.1021/ct4009848 | J. Chem. Theory Comput. 2014, 10, 805−815

Scheme 2. Representation of the Compounds Investigated Here[a]

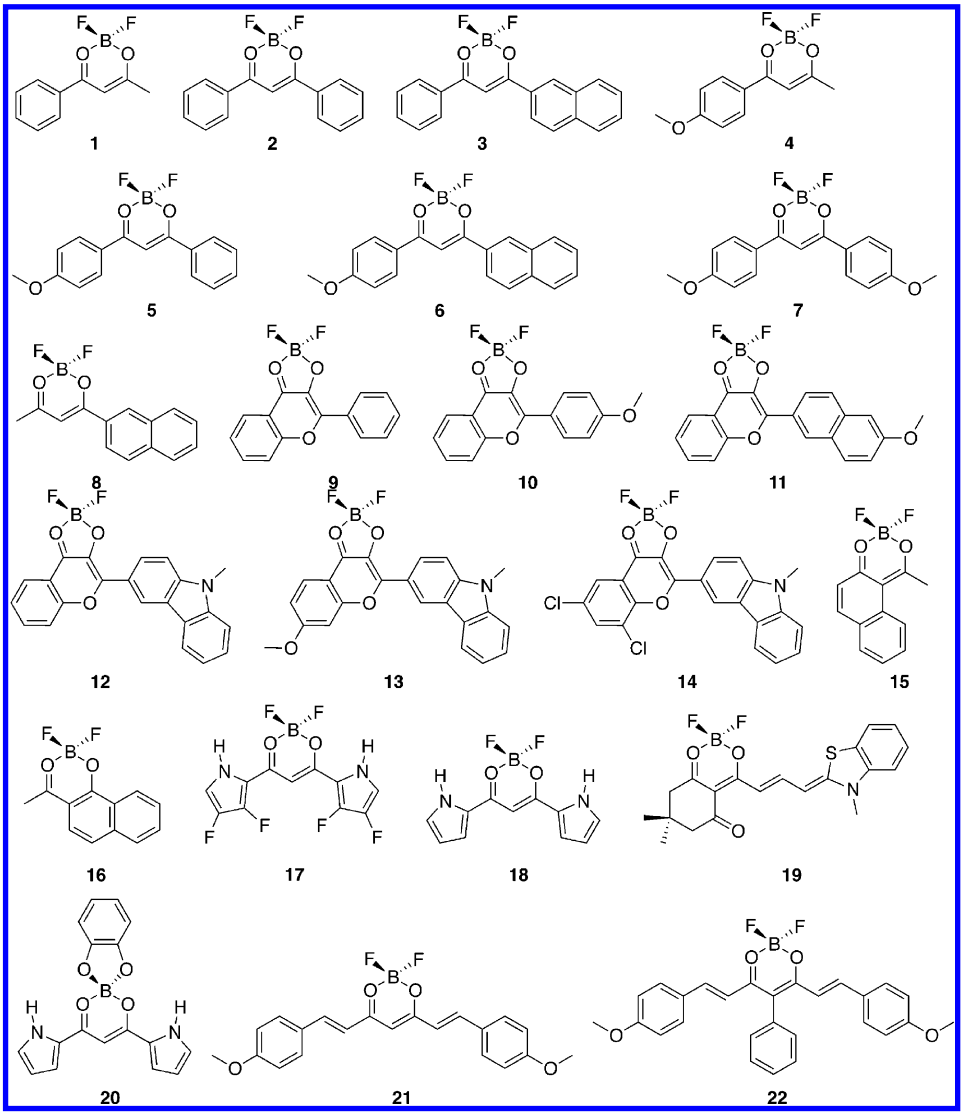

[a]The measured longest wavelength of absorption (λ_{abs}), emission wavelength (λ_{emi}), and solvents used, as well as the experimental references can be found in Table S-I in the Supporting Information (SI).

energies[55] of bis-aryl substituted dioxaborine, whereas the second and third works[24,25] were performed to estimate the π-electronic states of three OBO dyes.[56] In the present work, we investigate several solvent models derived from the Polarizable Continuum Model (PCM)[57] for computing the properties of OBO dyes, simulate the spectral signatures of a large panel of synthesized molecules and design red-shifted structures.

The paper is divided into three parts. First, we detail our computational procedure. Second, we present and discuss the results obtained with different methodologies with a focus on solvent models. Third, we focus on the analysis of cases of practical interest (auxochrome impact, vibronic shapes, dye design...).

2. METHODS

All calculations have been performed with the latest version of the *Gaussian 09* program package,[58] applying a tight self-consistent field convergence criterion (10^{-9} to 10^{-10}) a.u. and a strict optimization threshold (10^{-5} a.u. on average forces). The same DFT integration grid, namely the *ultrafine* pruned (99 590) grid, was used for all calculations. Optical signatures of the OBO dyes were simulated as follows. First, we optimized the geometries (R) of the ground states (GS) with DFT and determined the GS vibrations. The energies (E) of the electronically excited-states (ES) were next calculated at the TD-DFT level using these optimized GS geometries. The energy differences between the ES and the GS obtained in this way correspond to vertical absorption energies,

$$E^{\text{vert}-a} = E^{\text{ES}}(R^{\text{GS}}) - E^{\text{GS}}(R^{\text{GS}}) \quad (1)$$

For the record,[47,48] we note that these data cannot be rigorously compared to experimental λ_{max} of absorption, although such procedure might be effective in a homologous series of compounds. In a second stage, the optimized geometries of the first ES have been determined with TD-DFT using analytic gradients. The vertical transition energies calculated on the optimized ES geometry are the vertical fluorescence energies,

$$E^{\text{vert}-f} = E^{\text{ES}}(R^{\text{ES}}) - E^{\text{GS}}(R^{\text{ES}}) \quad (2)$$

dx.doi.org/10.1021/ct4009848 | J. Chem. Theory Comput. 2014, 10, 805−815

Table 1. Statistical Analysis for Dyes Shown in Scheme 2 Obtained with PCM-TD-M06-2X and PCM-TD-B3LYP Approaches[a]

functional	method	MSE	MAE	SD	R^2	max(+)	max(−)
B3LYP	E^{0-0} (LR,eq)	−0.149	0.170	0.133	0.826	0.121	−0. 556
	E^{0-0} (cLR,eq)	−0.053	0.234	0.290	0.601	0.452	−0.618
	E^{AFCP} (cLR,neq)	−0.090	0.274	0.358	0.501	0.450	−0.988
	E^{0-0} (SS,eq)	−0.294	0.424	0.516	0.387	0.375	−1.359
	E^{AFCP} (SS,neq)	−0.224	0.366	0.449	0.433	0.379	−1.162
M06-2X	E^{0-0} (LR,eq)	0.189	0.189	0.073	0.952	0.332	0.085
	E^{0-0}(cLR,eq)	0.411	0.411	0.086	0.927	0.585	0.193
	E^{AFCP} (cLR,neq)	0.414	0.414	0.087	0.926	0.587	0.193
	E^{0-0} (SS,eq)	0.298	0.316	0.162	0.784	0.565	−0.125
	E^{AFCP} (SS,neq)	0.367	0.367	0.137	0.828	0.596	0.049

[a]All values are given in eV except R^2.

The adiabatic energies, E^{adia}, are the difference of total electronic energies calculated for the two states in their respective minima. To calculate the 0−0 energies, E^{0-0}, the differences of the zero-point vibrational energy between the ES and the GS, ΔE^{ZPVE} were computed, and this required numerical differentiation for the ES. Of course, the vibrational frequency analysis were also used to check the nature of the stationary points of all states (true minima of the potential energy surface).

At this stage, it is important to state that we used the most widely applied continuum dielectric method, the PCM,[57] to model solvation effects. For ES, PCM has been applied in its linear response (LR),[59,60] corrected linear response (cLR)[61] and state specific (SS)[62] approaches considering both equilibrium (eq) and nonequilibrium (neq) limits that are adequate for slow and fast optical phenomena, respectively. Briefly, all the three models (LR, cLR, and SS) represent the solvent polarization in terms of induced charges on the surface of the cavity embedding the dye; however, the way this polarization changes with the electronic transition is differently introduced in these three schemes. Indeed, in the LR scheme the change in the PCM charges is calculated in terms of transition densities while in cLR this change is determined by the variation in the one-particle density matrix between the ground and the excited states obtained from the eigenvectors of the TD-DFT equations as well as from the solution of the Z-vector equation, which provides the orbital relaxation contribution. In the SS approach, a more complex iterative formulation is used in which the reference Kohn−Sham equation is also changed. These three models are thoroughly tested in the present work.

Best estimates (BE) of the 0−0 energies can be obtained combining a small atomic basis set (SBS), and a large atomic basis set (LBS), as well as several PCM models (LR, X: cLR or SS).[50,51] The 0−0 energies are equilibrium properties so that

$$E_{BE}^{0-0}(\mathrm{LR,\ eq}) = E_{LBS}^{adia}(\mathrm{LR,\ eq}) + \Delta E_{SBS}^{ZPVE}(\mathrm{LR,\ eq}) \quad (3)$$

$$E_{BE}^{0-0}(\mathrm{X,\ eq}) = E_{BE}^{0-0}(\mathrm{LR,\ eq}) + E_{SBS}^{adia}(\mathrm{X,\ eq}) - E_{SBS}^{adia}(\mathrm{LR,\ eq}) \quad (4)$$

Equation 4 implies additive cLR/SS and basis set effects, an approximation that has been demonstrated to be very accurate.[50,51] We underline that cLR and SS simulations are only possible as single point TD calculations and cannot be used to directly optimize ES geometries. The crossing point of absorption and emission bands corresponds to nonequilibrium phenomena in the experimental measurements. For this reason, the E^{0-0} has been corrected for nonequilibrium effects to reach E^{AFCP},

$$E^{AFCP}(X,\ \mathrm{neq}) = E_{BE}^{0-0}(X,\ \mathrm{eq}) + \frac{1}{2}[\Delta E_{neq/eq}^{vert-a}(X) + \Delta E_{neq/eq}^{vert-f}(X)] \quad (5)$$

where the correction term for the neq effects is composed of two parts,

$$\Delta E_{neq/eq}^{vert-a}(X) = E_{SBS}^{vert-a}(X,\ \mathrm{neq}) - E_{SBS}^{vert-a}(X,\ \mathrm{eq}) \quad (6)$$

$$\Delta E_{neq/eq}^{vert-f}(X) = E_{SBS}^{vert-f}(X,\ \mathrm{neq}) - E_{SBS}^{vert-f}(X,\ \mathrm{eq}) \quad (7)$$

We underline that in the LR scheme, fluorescence calculations are rather ill-defined, as the solvent response is not adapted to the real electronic density of the excited state as instead is done in the cLR or SS schemes. We redirect the interested readers to the original references 50, 52, and 53 for more details and discussions about this methodology. The results obtained for our set of OBO dyes are given in SI.

Vibrationally resolved spectra within the harmonic approximation were computed using the FCclasses program (FC).[63−65] The reported spectra were simulated using a convoluting Gaussian function presenting a half width at half-maximum (HWHM) that was adjusted to allow direct comparisons with experiments (typical value: 0.04 eV). A maximal number of 25 overtones for each mode and 20 combination bands on each pair of modes were included in the calculation. The maximum number of integrals to be computed for each class was first set to 10^6. In the cases where convergence of the FC factor [≥0.9] could not be achieved with this number of integrals, a larger value (10^{10}) was used so to overcome the 0.9 limit. Note that, in the following, the experimental fluorescence spectra measured in the wavelength scale have been transformed by applying an intensity correction proportional to ω^2 (the square frequency), in order to obtain line shapes that are directly comparable to theoretical data (the measured emission intensity physically decreasing by a factor of ω^2, which is not related to the vibronic couplings).[66] Indeed, this correction significantly affects the topology of the fluorescence spectra, contrary to other more negligible effects.[67]

As stated in the Introduction, TD-DFT is a powerful tool, but its use for real-life cases implies the choice of a specific exchange-correlation functional that plays key role on the accuracy of the final results. Previous benchmarks have shown that the M06-2X hybrid functional[68] stands as one of the best compromise for both vertical and 0−0 calculations of dyes,[50,69−71] and this is also true for the specific case of

dx.doi.org/10.1021/ct4009848 | J. Chem. Theory Comput. 2014, 10, 805−815

fluoroborate complexes.[51−53] For this reason, we have mainly chosen M06-2X and focused our methodological study on the three above-described PCM models. We also followed our recent results obtained for other fluoroborate dyes.[51−53,72] It was found that selecting 6-31G(d) as SBS is very effective for determining the geometrical and vibrational parameters, whereas a much more extended basis set, namely 6-311+G-(2d,p), can be used as LBS to obtain the basis set corrections through vertical TD-DFT calculations.

3. RESULTS AND DISCUSSION

3.1. 0−0 Energies. In this section, we aim to compare theoretical and experimental 0−0 energies. Experimental data refer to systems in dichloromethane with the exception of systems **15** (in chloroform) and **16** (in tetrahydrofuran). We have used the M06-2X hybrid functional[68] with five solvent approximations: LR,eq [0−0, eq 3], SS/cLR,eq [0−0, eq 4] and SS/cLR,neq [AFCP, eq 5], and we briefly evaluated the performance of B3LYP[73] and other functionals as well. Table 1 provides a statistical analysis for the OBO dyes displayed in Scheme 2: mean signed error (MSE), mean absolute error (MAE), standard deviation (SD), linear determination coefficient (R^2), as well as the maximal positive and negative deviations max(+) and max(−) are reported. The reader can find the 0−0 energies obtained with M06-2X and B3LYP for all dyes in the SI. The MSE is negative for B3LYP and becomes positive for M06-2X indicating that the experimental values are underestimated (overestimated) with the former (latter) functional, which is a rather common trend. Though B3LYP-(LR, eq) provides the smallest MAE (0.170 eV) and B3LYP(cLR,eq) the smallest MSE (−0.053 eV), respectively, this apparent accuracy comes with large SD and small R^2. In fact, M06-2X appears as a good compromise for OBO dyes. Indeed, one can find from Table 1 that M06-2X yields the largest correlation coefficient with 0.952 and the smallest SD (0.073 eV). This result nicely agrees with previous studies: M06-2X is very efficient to calculate the 0−0 energies of BODIPY and boranil dyes,[52,53] and this success also holds for cyanines.[74,75] In the following, we comment only the results obtained with M06-2X. For the records, note that the R^2 obtained for the same set of dyes is 0.897 with PBE0,[76] 0.943 with CAM-B3LYP[77] and 0.915 with ωB97X[78] [all in the (LR,eq) model], further justifying the choice of M06-2X.

Let us now discuss the impact of the solvent. Table 1 clearly indicates that marked differences between the three PCM models occur. Let us start by comparing LR and SS results. The LR model, in the equilibrium limit, obviously provides more consistent results than its SS counterpart. This is illustrated by the (LR, eq) R^2 of 0.952 that is much larger than the corresponding SS values of 0.784 (eq) and 0.828 (neq). Of course, this is reflected in the SD that exceeds 0.1 eV with the SS-M06-2X combination. Clearly, the SS-PCM model cannot reproduce the experimental trends for OBO dyes in a very satisfying way. This phenomenon was already noticed in a previous work[53] devoted to NBO dyes, and we refer the readers to it for further discussion.

With the cLR approach, we found that equilibrium and nonequilibrium limits provide relatively similar statistical data. Indeed, for SD (R^2), we obtain 0.086 eV (0.927) in the eq limit and 0.087 eV (0.926) in the neq limit: cLR provides a consistency with experiment that is similar to the LR one (the difference of R^2 between the two models being as small as 0.025). One therefore faces a dilemma: as discussed above, the LR model should be insufficient to correctly describe the ES polarization but nevertheless yields the smallest MAE. While this is not a result that can be easily explained, a general comment can aid in finding a possible rationalization. All the experimental data refer to low polar solvents, and we therefore should expect that a purely electrostatic model as PCM, in all its different LR, cLR, and SS versions, recovers only a part of the whole solvent effect as it neglects possible important solute−solvent nonelectrostatic interactions. It is true that here the focus is on 0−0 energies, that is, differences of energies for which error cancellations should apply; however, this is not always the case: for example, solvent dispersion effects are expected to significantly differ for ground and excited states, the latter being generally larger. As a result, the neglect of these nonelectrostatic effects should lead to systematic errors.[79,80] The fact that LR gives the smallest MAE could be justified by indicating that this scheme in which the solvent electrostatic response to the solute excitation is determined by a transition density and not by the real change in the state density fortuitously recovers part of the missing term. This analysis seems also to be supported by the fact that for all the investigated solutes cLR gives too large 0−0 energies, for example, coherently with a neglect of a dispersion effect, which should stabilize more the excited than the ground state and consequently reduce the 0−0 energies. In addition, LR always yields an overestimation, but the error is reduced from ca. 0.4 to ca. 0.2 eV (we note that for SS both positive and negative errors are found). At this stage, we have decided to mainly go on with cLR that emerged as the best compromise between physical robustness of the model and consistency of the results, but we also present LR values in the following. Clearly, an investigation of the *pros* and *cons* of all these PCM models, on a more diverse set of dyes would be welcome, but this is beyond our scope here.

Finally, we have performed calculations with M06-2X using the Tamm-Dancoff approximation (TDA). The TDA energies obtained with different solvent models and the related statistical analysis are collected in SI. The linear correlation coefficient (R^2) obtained with TDA are smaller than with TD-DFT: it ranges from 0.725 (AFCP) to 0.896 (LR,eq). We note that when moving from TD-DFT to TDA, irrespective of the selected PCM-approach, not only does R^2 decrease but also both MSE and MAE increase. TDA approach is derived from TD-DFT by discarding the deexcitation matrix from the working equations[81] and this is known to be a valid approximation for most cases but cyanine dyes constitute exceptions.[75] TDA was therefore not used further in the present contribution. In short, for 0−0 energies of OBO dyes, TD-DFT calculations combining the M06-2X functional to the LR-PCM/cLR-PCM models could be viewed as a reasonable choice.

3.2. Impact of the Auxochromes. Figures 1 and 2 illustrate the density difference plots for selected OBO dyes. In all cases, the two oxygen atoms participate in the excited-state, whereas the BF_2 contribution is rather small. A comparison between **2** and **18** (see Figure 1) indicates that the replacement of the phenyl rings by pyrrole rings induces a modest bathochromic shift due to the emergence of intramolecular H-bonds with the oxygen atoms, allowing the stabilization of the extra charge gained by these atoms in the excited-states. We computed a shift of +33 (+49) nm for the absorption and +17 (+32) nm for the emission with cLR (LR). The corresponding experimental values are +52 nm and +55 nm: the selected

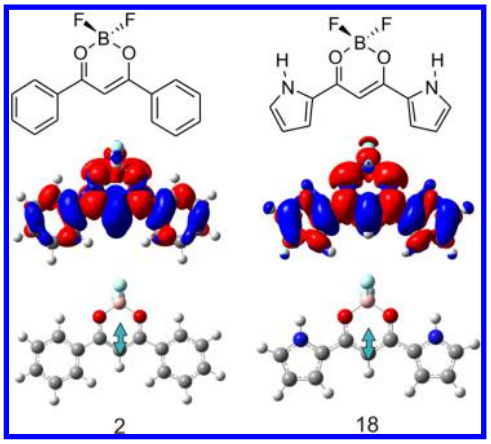

Figure 1. PCM-TD-M06-2X/6-31G(d) density difference plots for **2** (left) and **18** (right). The blue (red) zones indicate density decrease (increase) upon transition. At the bottom, the small dipolar CT vectors are displayed. The selected contour threshold is 0.0004 au.

approach reasonably reproduces this measured effect. Both **2** and **18** present rather small Stokes shifts, which respectively amount to 16 (37) nm and 19 (21) nm in experiment (theory). These small variations are consistent with the similar topologies of the density difference plots shown in Figure 1. Thanks to a recently developed approach,[82,83] one can quantify from the GS and ES densities the charge transfer (CT) distance (d^{CT}), the transferred charge (q^{CT}) and the CT dipole moment (μ^{CT}). **2** and **18** present similar q^{CT} of 0.42, 0.45 e and d^{CT} of 0.60, 0.69 Å, respectively (see Table 2). In other words, the CT distances, in this dipolar approximation, are small and the states can be regarded as $\pi \rightarrow \pi^*$ transitions. Indeed, in states having a large CT character, d^{CT} is often larger than ca. 2.0 Å.[82,83]

In Figure 2, the density difference plots of three OBO dyes having the same skeleton including a carbazole unit are given, while the CT parameters can be found in Table 2. When going from **12** to **13**, we calculated a very small hypsochromic shift of both absorption and emission bands of −2 (−2) nm and −4 (−7) nm at cLR (LR) level, in line with the experimental values of −4 nm and −11 nm, respectively. The carbazole acts as an electron donor (Figure 2), so adding a methoxy donor on the opposite site is detrimental for CT, and this reflects in the decrease of the ES dipole moment from **12** (18.45 D) to **13** (15.90 D). On the contrary, going from **12** (μ^{GS} = 11.73 D, μ^{ES} = 18.45 D) to **14** (μ^{GS} = 10.90 D, μ^{ES} = 20.00 D), provokes a

Table 2. CT Distance (d^{CT} in Å), Transferred Charge (q^{CT} in e), CT Dipole, and Ground/Excited State Dipole Moments (in Debye) for Selected Dyes

dye	d^{CT}	q^{CT}	μ^{CT}	μ^{GS}	μ^{ES}
2	0.60	0.42	1.20	9.30	10.50
18	0.69	0.45	1.40	6.00	7.40
12	3.40	0.63	6.72	11.73	18.45
13	3.10	0.60	4.40	11.50	15.90
14	3.60	0.66	9.10	10.90	20.00
19	1.11	0.40	2.04	13.05	15.09

bathochromic displacement of +21 (+21) nm for absorption and +22 (+19) nm for emission (in the line of the measurements of +24 nm and +37 nm, respectively), and this is related to the accepting character of the two chlorine atoms placed in meta position (mostly in red in Figure 2).

Finally, we have characterized one of the largest molecule of Scheme 2, namely **19**, that absorbs and emits at rather long wavelengths and is a good candidate for organic solar cell applications.[37] The density difference plots indicate a limited CT character (see the CT distance in Table 2) but a significant cyanine character with an alternating pattern on the polyene segment. The estimated Stokes shift of **19** is small, 20 nm, which is consistent with the experiment (14 nm). This section therefore illustrates that OBO structures can develop both CT and cyanine characters depending on the substitution pattern.

3.3. Vibronic Shapes. In this section, we compare the experimental and theoretical band shapes of selected dyes, as several OBO spectra presenting notable vibronic structures. Indeed, our computational protocol, PCM-TD-M06-2X, is expected to provide rather accurate optical band topologies, not only 0−0 energies. Vibrationally resolved absorption and emission bands for dyes **9**, **10**, **11**, **12**, **13**, and **14** obtained in dichloromethane are displayed in Figure 3. Vibronic spectra for other OBO dyes are available in the SI. One can see that when going from **9** (black) to **14** (cyan), absorption and emission band shapes are red-shifted, which is in agreement with experiment (see ref 43). It was observed that both **9** and **11** present significant structures in both their absorption and emission bands. For this reason, we display stick vibronic spectra in Figure 4. For **9**, the agreement between experimental and theoretical band shapes is satisfactory. For this molecule, the theoretical stick absorption spectrum is composed of several characteristic peaks, two intense being located at 814 and 1679 cm^{-1} relative to the 0−0 reference. These two peaks

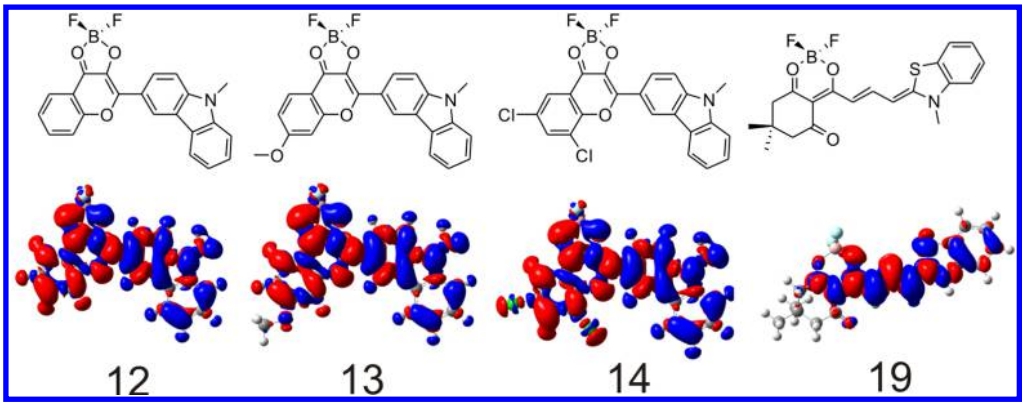

Figure 2. PCM-TD-M06-2X/6-31G(d) density difference plots for (from left to right) **12**, **13**, **14**, and **19**. The selected contour threshold is 0.0004 au.

dx.doi.org/10.1021/ct4009848 | J. Chem. Theory Comput. 2014, 10, 805−815

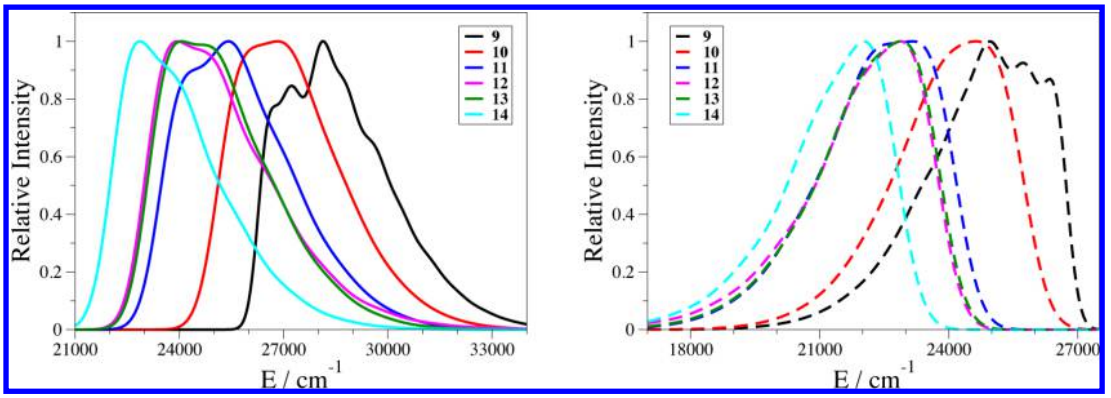

Figure 3. Absorption (left) and emission (right) band shapes of **9**, **10**, **11**, **12**, **13**, and **14** computed with M06-2X. The experimental spectra can be found in ref 43.

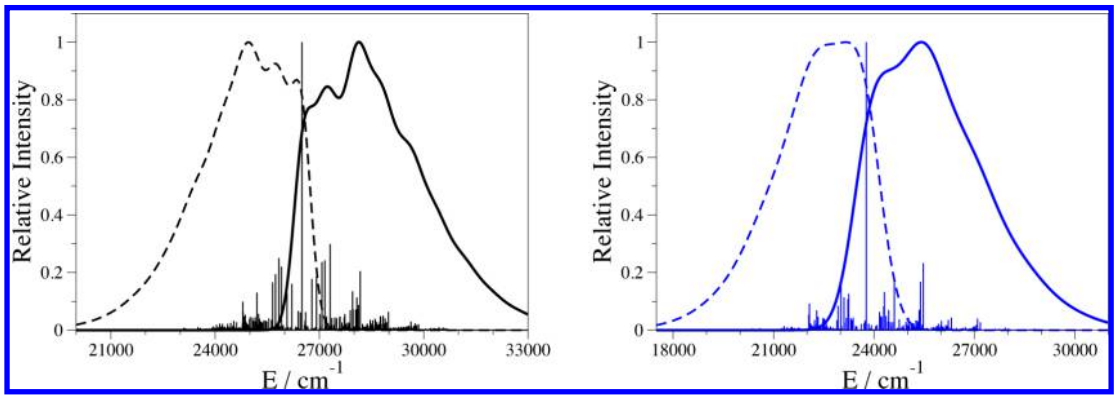

Figure 4. Absorption (full lines) and emission (dashed lines) spectra of **9** (left) and **11** (right) computed with M06-2X. The experimental spectra can be found in ref 43.

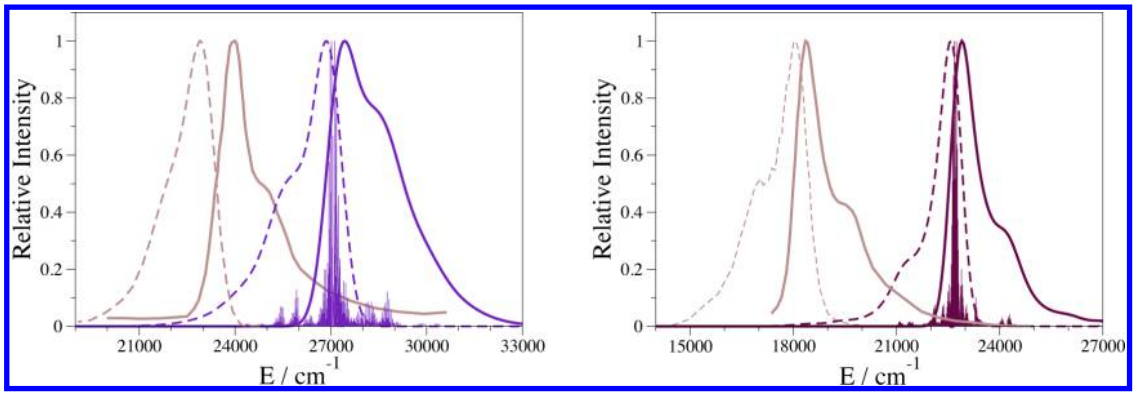

Figure 5. Theoretical (violet, indigo) and experimental (brown) spectra for absorption (full lines) and emission (dashed lines) of **17** (left) and **19** (right) computed with M06-2X. The experimental spectra are adapted with permission from refs 18 (copyright 2006, American Chemical Society) and 37 (Copyright 2011, Elsevier).

correspond to, on the one hand, an asymmetric stretching of the OBO and, on the other hand, to CC stretching localized on the two phenyl rings (see movies in the SI). For the emission, the three main vibrational modes contributing to the overall shape appear at 663, 1294, and 1698 cm^{-1}. These modes again correspond to stretching of the rings and of the OBO moiety (see movies in the SI). For **11**, we can distinguish two important vibrational GS modes at 834 and 1703 cm^{-1} accounting for the emission band shape. These modes correspond to the stretching of the OBO unit and the naphthalene, respectively (see movies in the SI).

Figure 5 provides the vibronic spectra of **17** and **19** with a direct comparison with measured spectra. For both absorption and emission bands, it is clear that theory provides an overall accurate reproduction of the experimental topologies, as the relative positions of all the peaks/shoulders are well restored except for the shift of the 0−0 band discussed previously. Indeed, the experimental spectra of **17** (**19**) presents an absorption shoulder at ca. 400 (500) nm and an emission shoulder at ca. 455 (575) nm, respectively. These shoulders have a ca. half intensity compared to the main peaks. Using PCM-TD-M06-2X, the height of the shoulders are slightly overrated for **17** and underrated for **19**. To gain insights in the

dx.doi.org/10.1021/ct4009848 | J. Chem. Theory Comput. 2014, 10, 805−815

nature of the vibrational modes present in these shoulders, we have plotted stick spectra (see Figure 5). Contrary to previous cases, the stick spectra of **17** and **19** present a large number of individual vibrational transitions of comparable intensity and one cannot distinguish a few isolated modes that could explain the band shape in a simple fashion.

3.4. Double BF_2 Complexes. So far, we have only used OBO dyes presenting one BF_2-chelating moiety. To the best of our knowledge, only Yamashita and co-workers,[24,25] have synthesized (three) OBO dyes with two BF_2-chelating moieties around a tetracene, a perylene, and an octafluorotetracene central core (see Figure 6). The 0−0 energies obtained with

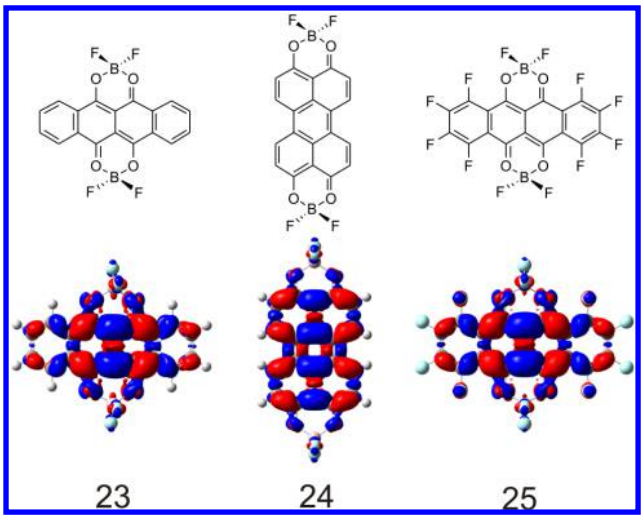

Figure 6. Representation of double BF_2 complexes based on tetracene (left, **23**), perylene (middle, **24**), and octafluorotetracene (right, **25**) fused cores.

different solvent models and the M06-2X hybrid functional are listed in Table S-VI in the SI, whereas Figures 7 and 8 provide vibronic spectra of tetracene (**23**), perylene (**24**) and octafluorotetracene (**25**) compounds. These dyes absorb and emit at rather long wavelengths compared to other OBO structures. The absorption bands are located between 420 and 470 (520−575) nm and the emission maxima take place in the 490−520 (520−570) nm region in theory (experiment), illustrating once more that the transition energies are overestimated by theory, although the trends when going

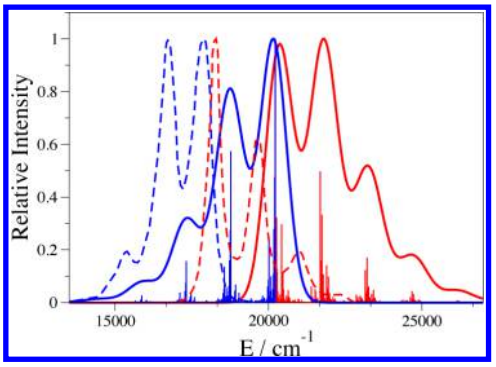

Figure 8. Experimental (dashed lines) and theoretical spectra (full lines) for absorption (red) and emission (blue) of **25**. The experimental spectra are adapted with permission from ref 25. Copyright 2009, American Chemical Society.

from one system to another are reasonably restored by TD-DFT.

The calculated Stokes shifts of both **23** and **24** dyes are very small (6 and 4 nm, respectively, with cLR), whereas the corresponding experimental values attain 6 nm for (**23**) and 3 nm for (**24**). These values are, in fact, comparable to the values measured for DHND (10 nm) and tetracene (4 nm), indicating that the **23** and **24** rigid chromophores are not significantly affected by the presence of the BF_2 groups. This is consistent with the reorganization of the electronic density (see Figure 6), which clearly corresponds to symmetric $\pi \rightarrow \pi^*$ transitions centered on the hydrocarbon cores. For **23** and **24**, we can distinguish a few key vibrational modes for both absorption and emission curves (see Figure 7). We note that the band shapes of these two dyes are slightly red-shifted relative to DHND or tetracene moieties but do conserve the same topology. For the absorption (emission) of **23**, the second maximum mainly implies one vibrational mode located at 1532 (1392) cm^{-1} (see stick spectra). These modes are shown in the SI and correspond to the stretching of the two central rings and of the full molecule, respectively.

The octafluorotetracene compound, **25**, is characterized by a larger electron affinity than the two other structures due to the enhancement of its quadrupolar nature by fluorination (see Figure 6). When going from **23** to **25**, the replacement of the hydrogen atoms by fluorine atoms induces a red-shift. We compute a modest bathochromic shift of +23 (+31) nm for the emission, which slightly underrates the experimental reference

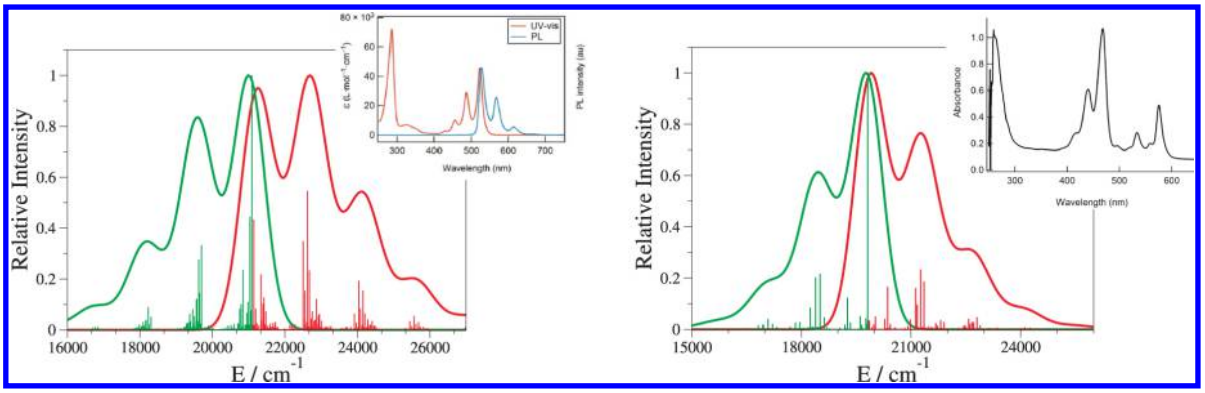

Figure 7. Convoluted and stick spectra of the absorption (red) and emission (green) of **23** (left) and **24** (right). The experimental absorption and emission spectra for **23** and the experimental absorption spectra for **24** (the insets) are both reproduced with permission from ref 24. Copyright 2009, American Chemical Society.

dx.doi.org/10.1021/ct4009848 | J. Chem. Theory Comput. 2014, 10, 805−815

Scheme 3. Representation of New Chromophores

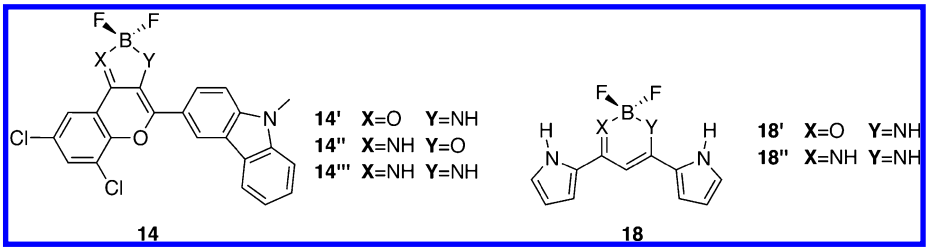

(see Figure 8). The second most intense contributions in the stick spectra, explaining the second maxima, correspond to modes at 1468 and 1451 cm^{-1} for absorption and emission, respectively (see movies in the SI).

3.5. Further Discussions. As mentioned in the Introduction, BODIPY, aza-BODIPY, and boranil dyes have attracted a widespread interest due to their remarkable properties. For this reason, we have designed new fluorophores that are based on **14** and **18** (see Scheme 3) and assessed the impact of replacing the OBO sequence by OBN and NBN sequences. The 0−0 energies obtained in dichloromethane can be found in SI. Vibrationally resolved absorption and emission bands for **14** and **14′** are also displayed in the SI. The simulated spectra of **18**, **18′**, and **18″** (Figure 9) show successive displacements of

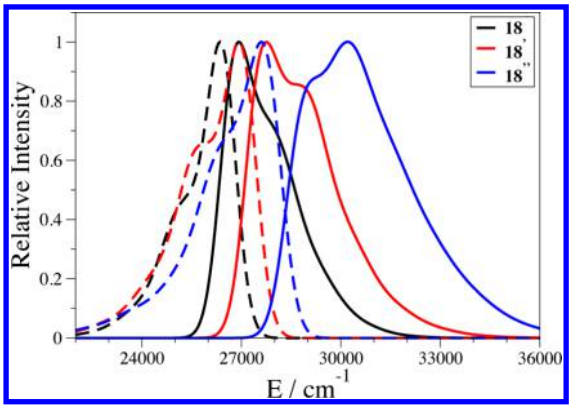

Figure 9. Absorption (full lines) and emission (dashed lines) spectra computed for **18**, **18′**, and **18″**.

both absorption and emission bands to smaller wavelengths. Indeed, going from **18** to **18′**, that is replacing OBO by OBN induces modest hypsochromic shifts for both absorption −15 (−25) nm, and emission −7 (−17) nm, with cLR (LR). Interestingly, **18″** that presents the NBN sequence is shifted hypsochromically by −31 (−46) nm compared to **18**, so that the variations are not additive when changing one or two oxygen atoms. We underline that **18″** presents a larger Stokes shift (35 nm) than the other structures. On the contrary, **14‴**, with the NBN sequence, undergoes a shift to longer wavelengths compared to **14**. The AFCP energies indeed decrease in the order: **14″** > **14** > **14‴** > **14′**, indicating that NBN-bidentate ligand might also induce bathochromic shift in some cases. It might look counterintuitive that the transition energies of the two NBO structures are not in between their OBO and NBN counterparts. However, as can be seen in Figure 4, the **X** and **Y** atoms undergo contrasted changes of density upon photon absorption, so that the symmetric architectures (OBO and NBN) logically yield to intermediate values of transition energies. Of course, placing the nitrogen on the donor side (and the oxygen atom on the accepting side) favors the decrease of the AFCP energy.

In the same vein, we have designed new chromophores using both electron donors and acceptors aiming to maximize the CT character of OBO dyes, or at least to shift the absorption maximum toward longer wavelengths. Figure 10 shows the density difference plots for five new chromophores, whereas the CT data are listed in Table 3. Starting with the three first dyes presenting identical donor (NMe_2) and acceptor (CN) groups, one notices that the strongest CT character is obtained with **26** (see Table 3). Adding one or two thiophene rings in the central linker, does not imply a larger CT, as the excited state starts to become a $\pi \rightarrow \pi^*$ state localized on the central unit and, less and less implies the terminal groups. This phenomenon was already noticed for other families of push−pull systems.[84] Indeed, for **28** with two thiophenes (see top of Figure 10), the dimethylamino group does not play any role in the optical transition. The corresponding CT distance for **27** and **28** are 1.30 and 1.17 Å, respectively, that is much smaller than in **26** (3.35 Å). In short, increasing the π−conjugation cannot provide an important CT character consistently with previous investigations on push−pull molecules.[84]

Aiming to induce large bathochromic shift with OBO dyes, we have used an alternative strategy, by keeping the central OBO unit constant but expanding the side chains. This leads to **29** and **30** that are based on **18** (see bottom of Figure 10). Figure 1 and Figure 10 demonstrate that **18**, **29**, and **30** possess almost the same excited state topologies with a CT going from the pyrrole groups to the OBO center. With cLR (LR) approach, the 0−0 energies are 3.297 (2.945), 2.622 (2.339), and 2.328 (2.138) eV, for **18**, **29**, and **30**, respectively. This corresponds to successive decreases of −0.675 (−0.606) and −0.294 (−0.201) eV, and hence, this strategy is much more effective than expanding the linker between one acceptor and one donor groups, if one aims designing NIR absorbers.

4. CONCLUSIONS

Using TD-DFT, we have computed the 0−0 energies and band shapes of a large panel of OBO dyes. We have first focused on assessing the adequacy of three environmental PCM models: LR, cLR and SS using both their equilibrium and non-equilibrium limits. It turns out that the SS-PCM approach is not efficient to simulate the spectral properties of OBO chromophores since it yields the least consistent data. On the contrary, the difference between LR and cLR is rather small in terms of correlation with experiment with the R^2 discrepancy not exceeding 0.025. However, it is worth to note that the LR−cLR difference is large in terms of absolute values. Indeed, the former approach provides data closer to experiment, but this effect is maybe due to a fortuitous cancellation between the error that LR approach introduces in treating the electrostatic effects and the error due to the neglect of nonelectrostatic

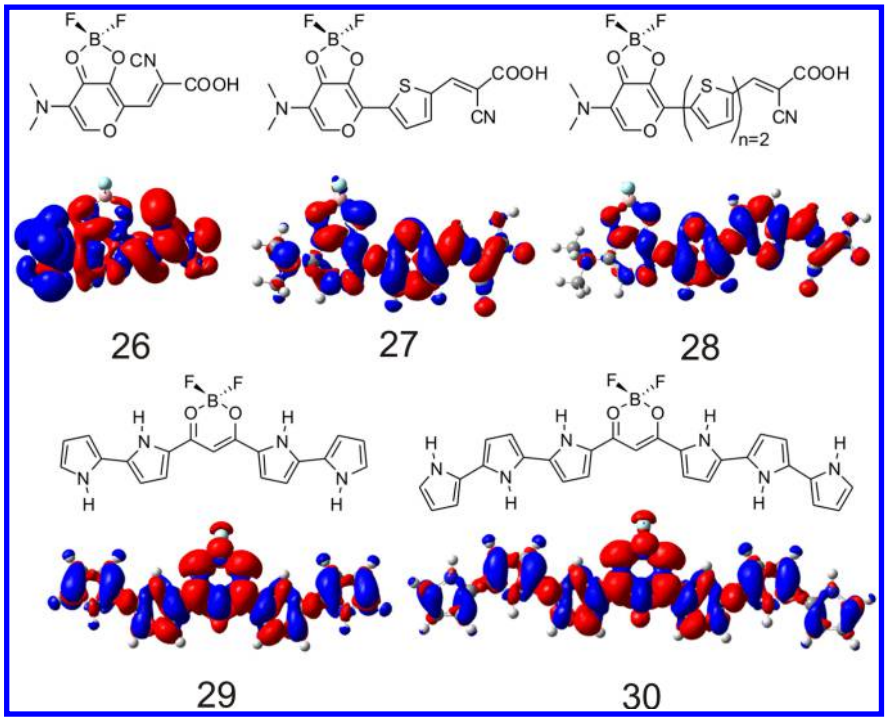

Figure 10. PCM-TD-M06-2X/6-31G(d) density difference plots for new chromophores: **26**, **27**, and **28** (top, from left to right), **29**, and **30** (bottom). The selected contour threshold is 0.0004 au.

Table 3. CT Parameters for the Dyes in Figure 10[a]

dye	d^{CT}	q^{CT}	μ^{CT}	μ^{GS}	μ^{ES}
26	3.35	0.73	7.69	16.04	23.73
27	1.30	0.45	2.50	9.50	12.00
28	1.17	0.47	2.02	6.15	8.17
29	3.44	0.64	0.78	9.87	10.63
30	1.39	0.40	0.95	5.40	6.35

[a]See caption of Table 2 for more details.

contributions. Part of the error can also be related to the difficulty of finding an exchange-correlation functional that reproduces the optical spectra of cyanine-like molecules with TD-DFT. Related to this partial cyanine nature, the TDA approximation of TD-DFT systematically provides poorer results for OBO dyes and is clearly not recommended. With the selected protocol, we could not only reproduce the experimental trends for 0–0 energies (with a R^2 of ca. 0.95) but also determine vibrationally resolved absorption and emission band shapes. They compare favorably with experiment for most tested compounds, and this also holds for the three available dyes presenting a double OBO-BF_2-chelation. In addition, we found that (1) replacing the OBO sequence by NBO or NBN might produce both bathochromic and hypsochromic shifts; (2) increasing the length of the π-conjugation linker between a push and a pull group does not systematically induce a stronger CT character; (3) extending the π-path around a central OBO unit acting as an acceptor is the fastest track to red-shift absorption and emission.

■ ASSOCIATED CONTENT

Supporting Information

List of solvents, experimental absorption, and emission values; 0–0 energies with different solvent models for all compounds, extra vibronic analysis, additional density difference plots; movies of vibrational modes. This material is available free of charge via the Internet at http://pubs.acs.org/.

■ AUTHOR INFORMATION

Corresponding Authors

*E-mail: benedetta.mennucci@unipi.it.
*E-mail: Boris.leguennic@univ-rennes1.fr.
*E-mail: Denis.Jacquemin@univ-nantes.fr.

Notes

The authors declare no competing financial interest.

■ ACKNOWLEDGMENTS

S.C. and A.C.E. thank the European Research Council (ERC, Marches 278845) for their PhD and postdoctoral grants. D.J. acknowledges the European Research Council (ERC) and the Région des Pays de la Loire for financial support in the framework of a Starting Grant (Marches 278845) and a *recrutement sur poste stratégique*, respectively. B.M. thanks the ERC for financial support in the framework of the Starting Grant (EnLight 277755). This research used resources of the GENCI-CINES/IDRIS (Grants c2013085117 and x2013080649), CCIPL (Centre de Calcul Intensif des Pays de Loire), and a local Troy cluster.

■ REFERENCES

(1) Loudet, A.; Burgess, K. *Chem. Rev.* **2007**, *107*, 4891–4932.
(2) Ulrich, G.; Ziessel, R.; Harriman, A. *Angew. Chem., Int. Ed.* **2008**, *47*, 1184–1201.
(3) Frath, D.; Azizi, S.; Ulrich, G.; Retailleau, P.; Ziessel, R. *Org. Lett.* **2011**, *13*, 3414–3417.
(4) Coskun, A.; Yilmaz, M.; Akkaya, E. U. *Org. Lett.* **2007**, *9*, 607–609.
(5) Murtagh, J.; Frimannsson, D. O.; O'Shea, D. F. *Org. Lett.* **2009**, *11*, 5386–5389.
(6) Zheng, Q.; Xu, G.; Prasad, P. *Chem.—Eur. J.* **2008**, *14*, 5812–5819.

(7) Killoran, J.; Allen, L.; Gallagher, J. F.; Gallagher, W. M.; O'Shea, D. F. *Chem. Commun.* **2002**, 1862−1863.
(8) Frangioni, J. V. *Curr. Opin. Chem. Biol.* **2003**, *7*, 626−634.
(9) Kuimova, M. K.; Botchway, S. W.; Parker, A. W.; Balaz, M.; Collins, H. A.; Anderson, H. L.; Suhling, K.; Ogilby, P. R. *Nature Chem.* **2009**, *1*, 69−73.
(10) Zhang, Z.; Achilefu, S. *Chem. Commun.* **2005**, 5887−5889.
(11) Chow, Y. L.; Johansson, C. I.; Zhang, Y.; Gautron, R.; Yang, L.; Rassat, A.; Yang, S. *J. Phys. Org. Chem.* **1996**, *9*, 7−16.
(12) Mirochnik, A. G.; Bukvetskii, B. V.; Gukhman, E. V.; Zhikhareva, P. A.; Karasev, V. E. *Russ. Chem. Bull.* **2001**, *50*, 1612−1615.
(13) Reutov, V. A.; Gukhman, E. V.; Kafitulova, E. E. *Russ. J. Gen. Chem.* **2003**, *73*, 1441−1444.
(14) Risko, C.; Zojer, E.; Brocorens, P.; Marder, S. R.; Brédas, J. L. *Chem. Phys.* **2005**, *313*, 151−157.
(15) Maeda, H.; Kusunose, Y. *Chem.—Eur. J.* **2005**, *11*, 5661−5666.
(16) Zyabrev, K. V.; Ilchenko, A. Y.; Slominskii, Y. L.; Romanov, N. N.; Tolmachev, A. I. *Dyes Pigm.* **2006**, *71*, 199−206.
(17) Fujimoto, C.; Kusunose, Y.; Maeda, H. *J. Org. Chem.* **2006**, *71*, 2389−2394.
(18) Maeda, H.; Ito, Y. *Inorg. Chem.* **2006**, *45*, 8205−8210.
(19) Fedorenko, E. V.; Mirochnik, A. G.; Karasev, V. E.; Bukvetskii, B. V. *Russ. J. Gen. Chem.* **2006**, *80*, 2192−2195.
(20) Zhang, G.; Chen, J.; Payne, S. J.; Kooi, S. E.; Demas, J. N.; Fraser, C. L. *J. Am. Chem. Soc.* **2007**, *129*, 8942−8943.
(21) Gwengo, F. P. M. C.; Lindeman, S. V.; Smith, M. D.; Gardinier, J. R. *Eur. J. Inorg. Chem.* **2008**, *20*, 3200−3211.
(22) Zyabrev, K.; Doroshenko, A.; Mikitenko, E.; Slominskii, Y.; Tolmachev, A. *Eur. J. Org. Chem.* **2008**, 1550−1558.
(23) Ran, C.; Xu, X.; Raymond, S. B.; Ferrara, B. J.; Neal, K.; Bacskai, B. J.; Medarova, Z.; Moore, A. *J. Am. Chem. Soc.* **2009**, *131*, 15257−15261.
(24) Ono, K.; Yamaguchi, H.; Taga, K.; Saito, K.; Nishida, J.; Yamashita, Y. *Org. Lett.* **2009**, *11*, 149−152.
(25) Ono, K.; Hashizume, J.; Yamaguchi, H.; Tomura, M.; Nishida, J.; Yamashita, Y. *Org. Lett.* **2009**, *11*, 4326−4329.
(26) Kersey, F. R.; Zhang, G.; Palmer, G. M.; Dewhirst, M. W.; Fraser, C. L. *ACS Nano* **2010**, *4*, 4989−4996.
(27) Zhang, G.; Lu, J.; Fraser, C. L. *Inorg. Chem.* **2010**, *49*, 10747−10749.
(28) Maeda, H.; Bando, Y.; Haketa, Y.; Honsho, Y.; Seki, S.; Nakajima, H.; Tohnai, N. *Chem.—Eur. J.* **2010**, *16*, 10994−11002.
(29) Maeda, H.; Takayama, M.; Kobayashic, K.; Shinmori, H. *Org. Biolmol. Chem.* **2010**, *8*, 4308−4315.
(30) Fedorenko, E. V.; L'vov, I. B.; Vovna, V. I.; Shlyk, D. K.; Mirochnik, A. G. *Russ. Chem. Bull* **2010**, *59*, 1041−1046.
(31) Liu, T.; Chien, A. D.; Lu, J.; Zhang, G.; Fraser, C. L. *J. Mater. Chem.* **2011**, *21*, 8401−8408.
(32) Gerasov, A. O.; Zyabrev, K. V.; Shandura, M. P.; Kovtun, Y. P. *Dyes Pigm.* **2011**, *89*, 76−85.
(33) Zhang, G.; Singer, J. P.; Kooi, S. E.; Evans, R. E.; Thomas, E. L.; Fraser, C. L. *J. Mater. Chem.* **2011**, *21*, 8295−8299.
(34) Maeda, H.; Kitaguchi, K.; Haketa, Y. *Chem. Commun.* **2011**, *47*, 9342−9344.
(35) Nguyen, N. D.; Zhang, G.; Lu, J.; Shermana, A. E.; Fraser, C. L. *J. Mater. Chem.* **2011**, *21*, 8409−8415.
(36) Haketa, Y.; Sakamoto, S.; Chigusa, K.; Nakanishi, T.; Maeda, H. *J. Org. chem.* **2011**, *76*, 5177−5184.
(37) Zyabrev, K.; Dekhtyar, M.; Vlasenko, Y.; Chernega, A.; Slominskii, Y.; Tolmachev, A. *Dyes Pigm.* **2011**, *92*, 749−757.
(38) Vovna, V. I.; Kazachek, M. V.; L'vov, I. B. *Opt. Spectro.* **2012**, *112*, 497−505.
(39) Felouat, A.; D'Aléo, A.; Fages, F. *J. Org. Chem.* **2013**, *78*, 4446−4455.
(40) Glotzbach, C.; Kauscher, U.; Voskuhl, J.; Kehr, N. S.; Stuart, M. C. A.; Frohloch, R.; Galla, H. J.; Ravoo, B. J.; Nagura, K.; Saito, S.; Yamaguchi, S.; Wurthwein, E. U. *J. Org. Chem.* **2013**, *78*, 4410−4418.
(41) Xu, S.; Evans, R. E.; Liu, T.; Zhang, G.; Demas, J. N.; Trindle, C. O.; Fraser, C. L. *Inorg. Chem.* **2013**, *52*, 3597−3610.
(42) Chambon, S.; D'Aléo, A.; Baffert, C.; Wantza, G.; Fages, F. *Chem. Commun.* **2013**, *49*, 3555−3557.
(43) D'Aléo, A.; Fages, F. *Photochem. Photobiol. Sci.* **2013**, *12*, 500−510.
(44) Maeda, H.; Hane, W.; Bando, Y.; Terashima, Y.; Haketa, Y.; Shibaguchi, H.; Kawai, T.; Naito, M.; Takaishi, K.; Uchiyama, M.; Muranaka, A. *Chem.—Eur. J.* **2013**, *19*, 16263−16271.
(45) Casida, M. E. In *Time-Dependent Density-Functional Response Theory for Molecules*; Chong, D. P., Ed.; Recent Advances in Density Functional Methods; World Scientific: Singapore, 1995; Vol. *1*; pp 155−192.
(46) Jacquemin, D.; Mennucci, B.; Adamo, C. *Phys. Chem. Chem. Phys.* **2011**, *13*, 16987−16998.
(47) Goerigk, L.; Moellmann, J.; Grimme, S. *Phys. Chem. Chem. Phys.* **2009**, *11*, 4611−4620.
(48) Goerigk, L.; Grimme, S. *J. Chem. Phys.* **2010**, *132*, 184103.
(49) Send, R.; Kühn, M.; Furche, F. *J. Chem. Theory Comput.* **2011**, *7*, 2376−2386.
(50) Jacquemin, D.; Planchat, A.; Adamo, C.; Mennucci, B. *J. Chem. Theory Comput.* **2012**, *8*, 2359−2372.
(51) Chibani, S.; Le Guennic, B.; Charaf-Eddin, A.; Maury, O.; Andraud, C.; Jacquemin, D. *J. Chem. Theory Comput.* **2012**, *8*, 3303−3313.
(52) Chibani, S.; Le Guennic, B.; Charaf-Eddin, A.; Laurent, A. D.; Jacquemin, D. *Chem. Sci.* **2013**, *4*, 1950−1963.
(53) Chibani, S.; Charaf-Eddin, A.; Le Guennic, B.; Jacquemin, D. *J. Chem. Theory Comput.* **2013**, *9*, 3127−3135.
(54) Barone, V.; Bloino, J.; Biczysko, M.; Santoro, F. *J. Chem. Theory Comput.* **2009**, *5*, 540−554.
(55) More precisely, they have used the B3LYP hybrid exchange-correlation functional and apolarized double-ζ atomic basis set.
(56) They have used the B3LYP hybrid exchange-correlation functional and the 6-31G(d) atomic basis set.
(57) Tomasi, J.; Mennucci, B.; Cammi, R. *Chem. Rev.* **2005**, *105*, 2999−3094.
(58) Frisch, M. J.; Trucks, G. W.; Schlegel, H. B.; Scuseria, G. E.; Robb, M. A.; Cheeseman, J. R.; Scalmani, G.; Barone, V.; Mennucci, B.; Petersson, G. A.; Nakatsuji, H.; Caricato, M.; Li, X.; Hratchian, H. P.; Izmaylov, A. F.; Bloino, J.; Zheng, G.; Sonnenberg, J. L.; Hada, M.; Ehara, M.; Toyota, K.; Fukuda, R.; Hasegawa, J.; Ishida, M.; Nakajima, T.; Honda, Y.; Kitao, O.; Nakai, H.; Vreven, T.; Montgomery, J. A., Jr.; Peralta, J. E.; Ogliaro, F.; Bearpark, M.; Heyd, J. J.; Brothers, E.; Kudin, K. N.; Staroverov, V. N.; Kobayashi, R.; Normand, J.; Raghavachari, K.; Rendell, A.; Burant, J. C.; Iyengar, S. S.; Tomasi, J.; Cossi, M.; Rega, N.; Millam, J. M.; Klene, M.; Knox, J. E.; Cross, J. B.; Bakken, V.; Adamo, C.; Jaramillo, J.; Gomperts, R.; Stratmann, R. E.; Yazyev, O.; Austin, A. J.; Cammi, R.; Pomelli, C.; Ochterski, J. W.; Martin, R. L.; Morokuma, K.; Zakrzewski, V. G.; Voth, G. A.; Salvador, P.; Dannenberg, J. J.; Dapprich, S.; Daniels, A. D.; Farkas, Ö.; Foresman, J. B.; Ortiz, J. V.; Cioslowski, J.; Fox, D. J. *Gaussian 09 Revision D.01. 2009*; Gaussian Inc.: Wallingford CT, 2009.
(59) Cammi, R.; Mennucci, B. *J. Chem. Phys.* **1999**, *110*, 9877−9886.
(60) Cossi, M.; Barone, V. *J. Chem. Phys.* **2001**, *115*, 4708−4717.
(61) Caricato, M.; Mennucci, B.; Tomasi, J.; Ingrosso, F.; Cammi, R.; Corni, S.; Scalmani, G. *J. Chem. Phys.* **2006**, *124*, 124520.
(62) Improta, R.; Scalmani, G.; Frisch, M. J.; Barone, V. *J. Chem. Phys.* **2007**, *127*, 074504.
(63) Santoro, F.; Improta, R.; Lami, A.; Bloino, J.; Barone, V. *J. Chem. Phys.* **2007**, *126*, 084509.
(64) Santoro, F.; Improta, R.; Lami, A.; Bloino, J.; Barone, V. *J. Chem. Phys.* **2007**, *126*, 184102.
(65) Santoro, F.; Lami, A.; Improta, R.; Bloino, J.; Barone, V. *J. Chem. Phys.* **2008**, *128*, 224311.
(66) Valeur, B. *Molecular Fluorescence: Principles and Applications*; Wiley-VCH: Weinheim, 2002. pp 1−250.
(67) Avila Ferrer, F. J.; Cerezo, J.; Stendardo, E.; Improta, R.; Santoro, F. *J. Chem. Theory Comput.* **2013**, *9*, 2072−2082.

(68) Zhao, Y.; Truhlar, D. G. *Theor. Chem. Acc.* **2008**, *120*, 215−241.
(69) Charaf-Eddin, A.; Planchat, A.; Mennucci, B.; Adamo, C.; Jacquemin, D. *J. Chem. Theory Comput.* **2013**, *9*, 2749−2760.
(70) Isegawa, M.; Peverati, R.; Truhlar, D. G. *J. Chem. Phys.* **2012**, *137*, 244104.
(71) Leang, S. S.; Zahariev, F.; Gordon, M. S. *J. Chem. Phys.* **2012**, *136*, 104101.
(72) Le Guennic, B.; Chibani, S.; Charaf-Eddin, A.; Massue, J.; Ziessel, R.; Ulrich, G.; Jacquemin, D. *Phys. Chem. Chem. Phys.* **2013**, *15*, 7534−7540.
(73) Becke, A. D. *J. Chem. Phys.* **1993**, *98*, 5648−5652.
(74) Jacquemin, D.; Zhao, Y.; Valero, R.; Adamo, C.; Ciofini, I.; Truhlar, D. G. *J. Chem. Theory Comput.* **2012**, *8*, 1255−1259.
(75) Moore, B., III; Autschbach, J. *J. Chem. Theory Comput.* **2013**, *9*, 4991−5003.
(76) Adamo, C.; Barone, V. *J. Chem. Phys.* **1999**, *110*, 6158−6170.
(77) Yanai, T.; Tew, D. P.; Handy, N. C. *Chem. Phys. Lett.* **2004**, *393*, 51−56.
(78) Chai, J. D.; Head-Gordon, M. *J. Chem. Phys.* **2008**, *128*, 084106.
(79) Weijo, V.; Mennucci, B.; Frediani, L. *J. Chem. Theory Comput.* **2010**, *6*, 3358−3364.
(80) Marenich, A. V.; Cramer, C. J.; Truhlar, D. G. *J. Chem. Theory Comput.* **2013**, *9*, 3649−3659.
(81) Dreuw, A.; Head-Gordon, M. *Chem. Rev.* **2005**, *105*, 4009−4037.
(82) Le Bahers, T.; Adamo, C.; Ciofini, I. *J. Chem. Theory Comput.* **2011**, *7*, 2498−2506.
(83) Jacquemin, D.; Le Bahers, T.; Adamo, C.; Ciofini, I. *Phys. Chem. Chem. Phys.* **2012**, *14*, 5383−5388 Code available at Université de Nantes, http://www.sciences.univ-nantes.fr/CEISAM/erc/marches/ (accessed Aug. 6, 2012).
(84) Ciofini, I.; Le Bahers, T.; Adamo, C.; Odobel, F.; Jacquemin, D. *J. Phys. Chem. C* **2012**, *116*, 11946−11955.